Journal of Power Sources 195 (2010) 4290–4296

Contents lists available at ScienceDirect

Journal of Power Sources

journal homepage: www.elsevier.com/locate/jpowsour

Sol–gel synthesis of multiwalled carbon nanotube-$LiMn_2O_4$ nanocomposites as cathode materials for Li-ion batteries

Xian-Ming Liu[a,d], Zheng-Dong Huang[a], Seiwoon Oh[a], Peng-Cheng Ma[a], Philip C.H. Chan[b], Ganesh Kumar Vedam[c], Kisuk Kang[c], Jang-Kyo Kim[a,*]

[a] Department of Mechanical Engineering, Hong Kong University of Science & Technology, Clear Water Bay, Kowloon, Hong Kong, PR China
[b] Department of Electronic and Computer Engineering, Hong Kong University of Science & Technology, Clear Water Bay, Kowloon, Hong Kong, PR China
[c] Department of Materials Science and Engineering, Korea Advanced Institute of Science and Technology, 335 Gwahangno, Yuseong-gu, Daejeon 305-701, Republic of Korea
[d] College of Chemistry and Chemical Engineering, Luoyang Normal University, Luoyang City, 471022 Henan, PR China

ARTICLE INFO

Article history:
Received 17 September 2009
Received in revised form 9 December 2009
Accepted 3 January 2010
Available online 2 February 2010

Keywords:
Li-ion battery
Nanocomposite
Multiwalled carbon nanotube
Cyclic performance
Discharge capacity

ABSTRACT

This study reports the development of multiwalled carbon nanotube (MWCNT)-$LiMn_2O_4$ nanocomposites by a facile sol–gel method. The elemental compositions, surface morphologies and structures of the nanocomposites are characterized with a view to their use as cathode materials for Li-ion batteries. The results indicate that the nanocomposite consists of $LiMn_2O_4$ nanoparticles containing undamaged MWCNTs. The nanocomposites show high cycle performance with a remarkable capacity retention of 99% after 20 cycles, compared with $LiMn_2O_4$ nanoparticles with a 9% loss of the initial capacity after 20 cycles. Measurements of a.c. impedance show that the charge-transfer resistance of the nanocomposites is much lower than that of spinel $LiMn_2O_4$. A cyclic voltammetry study further confirms higher reversibility of the nanocomposites compared with $LiMn_2O_4$ particles. The enhanced electrochemical performance of the nanocomposites is attributed to the formation of conductive networks by MWCNTs that act as intra-electrode wires, thereby facilitating charge-transfer among the spinel $LiMn_2O_4$ particles.

1. Introduction

The demand for lithion-ion batteries (LIBs) with higher specific energy and higher power capacity for application in electric vehicles and power tools has led to a search for electrode materials with much higher electrochemical performance than conventional materials. Among all the commercially available devices, LIBs currently represent the state-of-the-art technology [1,2] in terms of high energy batteries, and they occupy a prime position in the market place for powering portable electronic devices such as laptops, personal digital assistants, and cellular phones. For use as power supplies for electric vehicles (EVs) and hybrid electric vehicles (HEVs), however, it is still a challenge to achieve the same high specific power using LIBs as is currently achieved with supercapacitors. In general, the power capability of LIBs is hindered by the kinetic problems of the electrode materials used. For high power (viz. high rates), the electrode materials in LIBs must possess a higher electronic/ionic conductivity and higher safety than those currently available.

Spinel $LiMn_2O_4$ has been studied extensively due to its potential use as a cathode material. In comparison with the conventional $LiCoO_2$ electrode, a cathode made from $LiMn_2O_4$ is much safer because of its higher thermal stability at the charged states, lower cost, contains more common elements, and is more in line with environmental standards [3,4]. For application in batteries, $LiMn_2O_4$ powder should consist of single-phase, homogeneous and uniform particles with a sub-micron size distribution and a large surface area in order to achieve excellent electrode properties. Although spinel $LiMn_2O_4$ has many advantages, its poor electrical conductivity has been considered a limiting factor for use in high-power applications. Another challenging issue with cathodes made of $LiMn_2O_4$ is that the capacity decays significantly with charge–discharge cycling, which has been a major problem prohibiting $LiMn_2O_4$ from commercial application [5]. This severe capacity fading is mainly due to the Jahn–Teller distortion at the surface of spinel $LiMn_2O_4$ [6–8], the dissolution of manganese in the electrolyte solution [9–11], the spinel $LiMn_2O_4$ with oxygen deficiency [12,13] and the decomposition of electrolyte solution at the electrode [14]. In order to enhance the cyclic performance of $LiMn_2O_4$, several strategies have been proposed, e.g., the partial substitution of mono-, di- or trivalent cations for Mn^{3+} [15,16] and coating the spinel $LiMn_2O_4$ particles themselves with inorganic compounds [17,18]. For example, Mg-doped

* Corresponding author. Tel.: +852 2358 5841; fax: +852 2358 1543.
E-mail address: mejkkim@ust.hk (J.-K. Kim).

0378-7753/$ – see front matter © 2010 Elsevier B.V. All rights reserved.
doi:10.1016/j.jpowsour.2010.01.068

spinel $LiMn_2O_4$ exhibited much improved cyclic performance [16]. Recently, spinel $LiMn_2O_4$ nanostructures (such as nanorods and nanowires) showed a very high cyclic performance and good capacity retention [19,20]. The studies were based on the experimental phase.

Multiwalled carbon nanotubes (MWCNTs), because of their unique one-dimensional tubular structure, high electrical conductivity and large surface area, have been considered an ideal nanomaterial to functionalize other materials for applications in energy conversion and storage. MWCNTs have been used as additive materials to improve the electrochemical characteristics of cathode materials, including $LiCoO_2$ and $LiFePO_4$ for Li-ion batteries [21–28]. MWCNTs are a good conducting agent that improves the electrical conduction and reversible capacity with a high cycle efficiency of cathode materials. Hybrid nanostructures composed of MWCNTs and oxide compounds, such as MWCNT-Co_3O_4 [29], MWCNT-TiO_2 [30] and MWCNT-Au/SnO_2 [31], have also been developed as anode materials. These hybrid materials possess not only the inherent properties of nanocrystals and MWCNTs acting alone, but also additional, unique properties that arise from the electrical and thermal interactions between them. In particular, the MWCNT additives can provide conducting networks that can, in turn, decrease the inner resistance of LIBs and thereby lead to higher specific capacities even at high charge–discharge current rates. Very few studies have hitherto been reported on the direct, sol–gel preparation of hybrid nanocomposites for cathode materials of LIBs. In this work, a new hybrid nanomaterial consisting of $LiMn_2O_4$ nanocrystals and MWCNTs is prepared using a facile sol–gel method followed by calcination at a low temperature. Its electrochemical performance as a cathode material for LIB is discussed.

2. Experimental

2.1. Synthesis of MWCNT-$LiMn_2O_4$ nanocomposites

MWCNTs used in this work were prepared by a chemical vapour grown method (supplied by Nanokarbon, Korea). The diameter and length ranged from 40 to 60 nm and 10 to 30 μm, respectively, according to the supplier's specification. The following reagents and solvent were used without further purification: lithium acetate dihydrate (99.999%, Sigma–Aldrich), manganese acetate tetrahydrate (99.99%, Sigma–Aldrich), methanol (>99.5%, Fisher), polyethylene glycol hexadecyl ether (Brij® 58, $M_n \sim 1124$, Sigma–Aldrich), and deionized water.

A typical procedure for the preparation of MWCNT-$LiMn_2O_4$ nanocomposites is shown in Fig. 1. 4 mmol of $LiCH_3COO{\cdot}2H_2O$ and 8 mmol of $Mn(CH_3COO)_2{\cdot}4H_2O$ were dissolved into 30 mL methanol with magnetic stirring at room temperature (designated S-A hereafter). A 20 mg sample of as-received MWCNTs was dispersed in methanol (30 mL) and 0.5 g of non-ionic surfactant (Brij® 58) was added and dissolved under ultrasonication treatment (designated S-B hereafter). The surfactant plays an important role in bridging the metal ions and the sidewalls of the MWCNTs as in polymer nanocomposites [32,33]. The MWCNT content was maintained at 10 wt.% of $LiMn_2O_4$. As a coordinating and combusting agent, 1.98 g of citric acid was added to 20 mL deionized water at room temperature. Then, S-A and S-B were added dropwise to the citric aqueous solution. The mixed solution was sonicated for 30 min to form a homogenous dispersion, which was then stirred and evaporated at 80 °C for 8 h. The resultant black mixtures were dried at 120 °C for 10 h to yield gel precursors. For the preparation of gel precursors, the molar ratio of citric acid to acetate ions was 0.25. Finally, these diverse gel precursors were calcined at 250 °C for 30 h in air, which were then cooled to room temperature naturally. $LiMn_2O_4$ powders without MWCNTs were also obtained by a similar process.

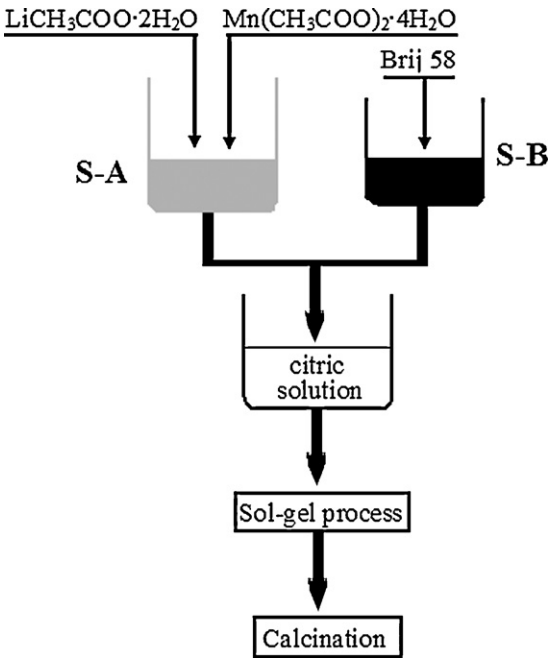

Fig. 1. Schematic of synthetic process for MWCNT-$LiMn_2O_4$ nanocomposites.

2.2. Assembly of coil-type cells

The electrochemical performance of the as-prepared powders was investigated using two-electrode coin-type cells (CR 2032) with lithium foil as a reference electrode. The working electrodes were assembled by coating the slurry of a mixture on an aluminum foil current-collector of 12 mm in diameter. The mixture was composed of 70 wt.% active material, 20 wt.% conducting agent (acetylene black) and 10 wt.% binder (polyvinylidene fluoride) in a N-methylpyrrolidinone (NMP) solvent. After drying in air at 80 °C for 4 h, the electrodes were pressed under a pressure of 7 MPa for 1 min, and then dried at 120 °C for 24 h in vacuum. The weight of the active materials was determined by weighing the Al foil before and after pressing the powders. The assembly process was carried out under a dry argon atmosphere in a glove box. The working electrode was used as the positive electrode and Li sheet as the negative electrode. The electrolyte was 1 M $LiPF_6$ dissolved in ethylene carbonate (EC):diethyl carbonate (DEC):ethyl methyl carbonate (EMC) at a 1:1:1 volume ratio. A polypropylene (PP) film (Cellgard 2400) was used as the separator.

2.3. Characterization

The phase structures of the $LiMn_2O_4$ nanoparticles and MWCNT-$LiMn_2O_4$ nanocomposites were determined by means of a powder X-ray diffraction (XRD) system (PW1830, Philips) with Cu Kα radiation (λ = 1.5406 Å) from 10° to 70° at a scanning rate of 2.0° s^{-1}. A field emission transmission electron microscope (FETEM, JEOL 2010F) was used to characterize the structural morphologies and the energy diffraction (ED) patterns. Scanning electron microscope (SEM, JEOL 6700F) images were taken to study the morphology of the synthesized products. X-ray photoelectron spectroscopy (XPS, Surface analysis PHI5600, Physical Electronics) was employed to evaluate the elemental compositions and chemical status of the samples using Al Kα line as the excitation source. The binding energy reference was taken at 284.7 eV for the C1s peak that arises

from surface hydrocarbons. Quantitative structural analysis of the nanocomposites was conducted on a RM3000 Micro Raman System (Renishaw PLC, UK) with argon laser excitation of 514 nm. Electrochemical impedance measurements were carried out in the frequency range between 100 kHz and 0.01 Hz, and the perturbation amplitude was controlled at 5 mV. Cyclic voltammetry and electrochemical impedance measurements were performed with a CHI660 electrochemical workstation. The galvanostatic charge–discharge characteristics of the cells were recorded with a LAND cell-testing system in the voltage range of 3.0–4.3 V (versus Li/Li^+) at room temperature.

3. Results and discussion

3.1. Structure and morphology

The X-ray diffraction patterns of $LiMn_2O_4$ nanoparticles and MWCNT-$LiMn_2O_4$ nanocomposites are presented in Fig. 2. The unit cell parameters and the volumes of $LiMn_2O_4$ calculated from the XRD data are consistent with the standard values (a_0 = 8.247 Å, V_0 = 560.90 Å^3) of JCPDS 35-0782. The XRD patterns of the $LiMn_2O_4$ nanoparticles present eight characteristic peaks at 18.6°, 36.4°, 38.3°, 44.3°, 48.5°, 58.6°, 64.2° and 67.8° that correspond to crystal planes of (1 1 1), (3 1 1), (2 2 2), (4 0 0), (3 3 1), (5 1 1), (4 4 0) and (5 3 1), respectively. For the nanocomposites, the characteristic peak at 2θ = 26.3° arising from the MWCNTs was not detected probably because of the small quantity of MWCNTs used and the overwhelming diffraction signals from the spinel $LiMn_2O_4$ phase.

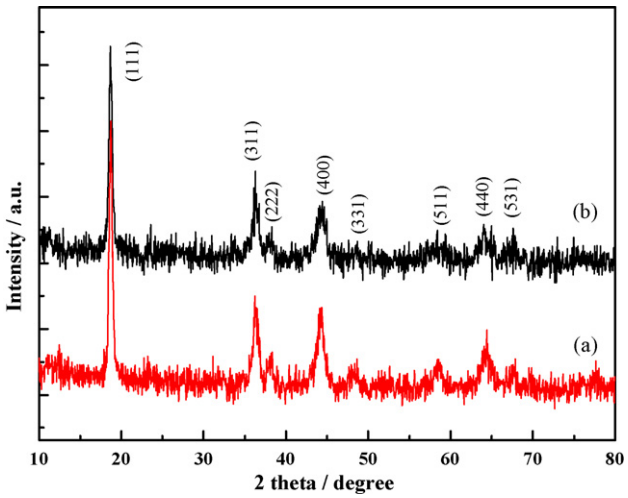

Fig. 2. XRD patterns of samples prepared by sol–gel method (a) without MWCNTs and (b) with MWCNTs.

The surface morphologies of the materials are shown in Fig. 3. $LiMn_2O_4$ consists of agglomerated nanoparticles with a fairly uniform individual particle diameter of 20–40 nm. The nanocomposite contains undamaged MWCNTs that are randomly mixed with $LiMn_2O_4$ nanoparticles. The TEM image (Fig. 4a) reveals that the surfaces of the MWCNTs are coated with a layer of spinel

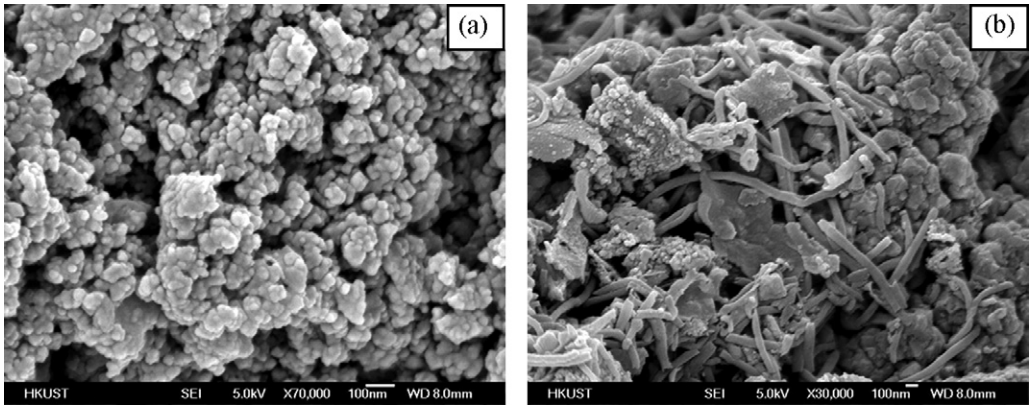

Fig. 3. SEM images of samples prepared by sol–gel method (a) without MWCNTs and (b) with MWCNTs.

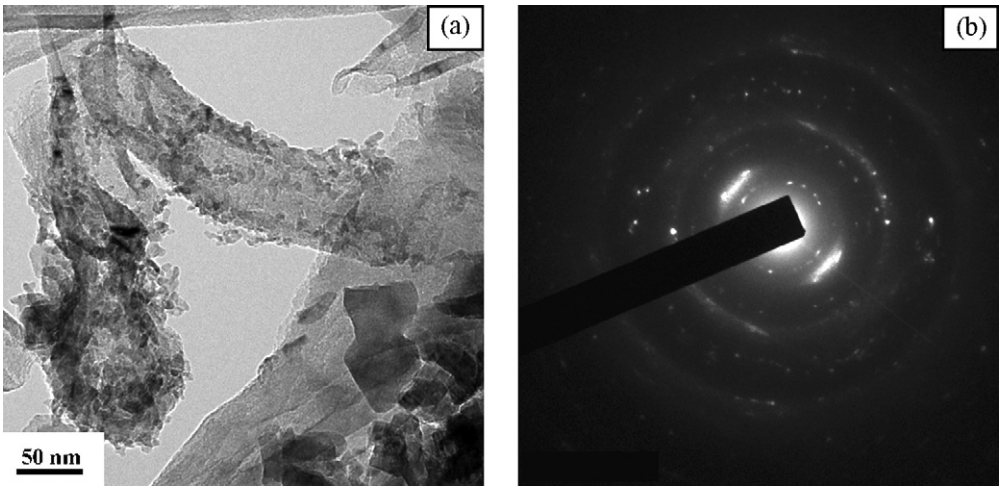

Fig. 4. TEM photograph (a) and ED pattern (b) of MWCNT-$LiMn_2O_4$ nanocomposites prepared by sol–gel method.

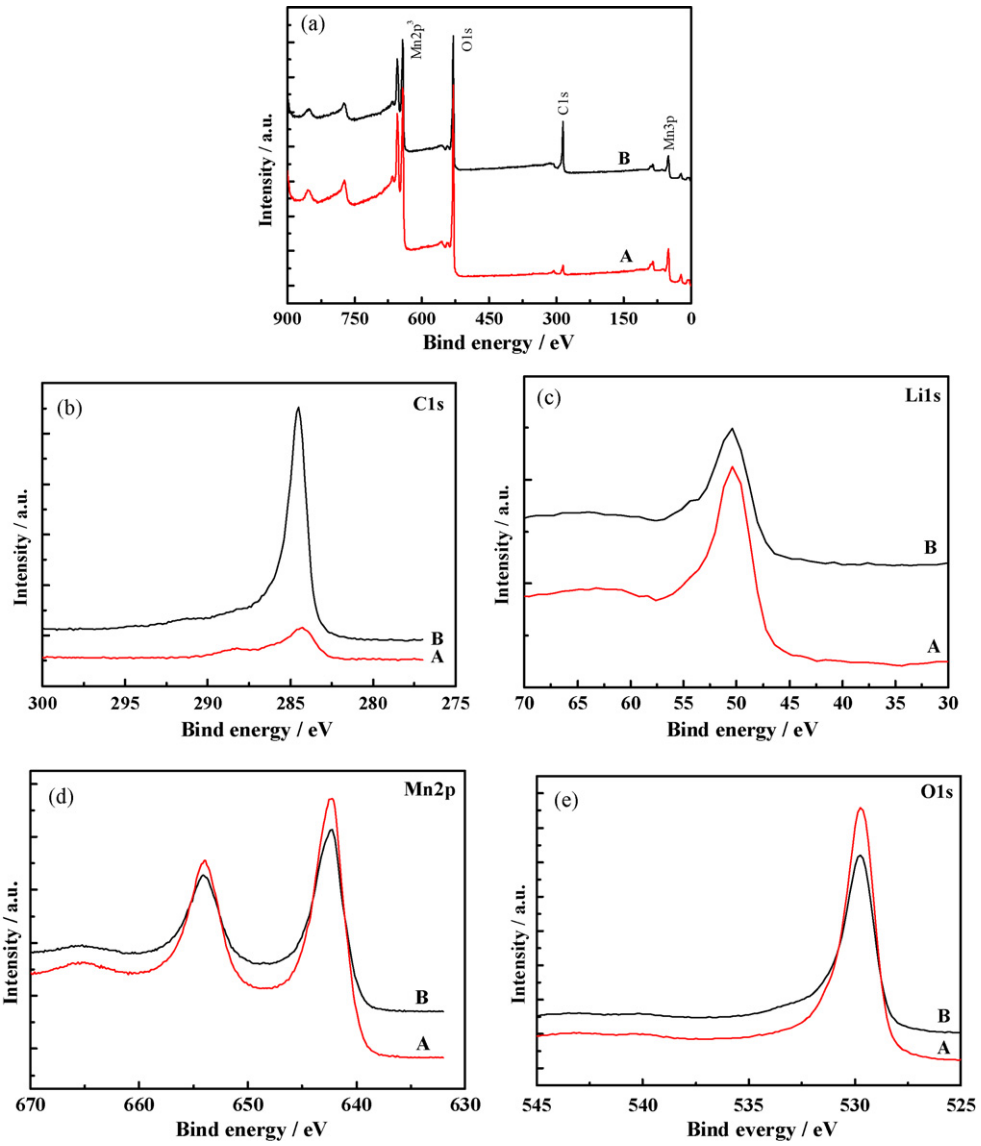

Fig. 5. XPS spectra of samples. (a) $LiMn_2O_4$ and (b) MWCNT-$LiMn_2O_4$ nanocomposites.

$LiMn_2O_4$ nanoparticles. The ED pattern (Fig. 4b) confirms that sound crystalline $LiMn_2O_4$ nanoparticles are successfully formed through the sol–gel process and calcination at a low temperature, which is in good agreement with the results from the XRD analysis.

3.2. Elemental compositions

The chemical compositions of the materials were characterized by XPS analysis. The survey XPS spectra shown in Fig. 5a indicate the signals of C, Li, Mn and O. For the $LiMn_2O_4$ nanoparticles, the signal of C is also detected at 284.8 eV, which is assigned to the ubiquitous adventitious carbon and is taken as a reference. For the nanocomposites, the signal of C arises from MWCNTs (Fig. 5b). The XPS spectra of Li1s, Mn2p and O1s core levels are shown in Fig. 5c–e, respectively. The peak of Li1s is located at 50.5 eV with a relatively low intensity, which indicates that lithium metal exists in the form of Li^+. The binding energy of $Mn2p^{3/2}$ is known to appear at 642.6 eV for Mn^{4+} in $LiMn_2{}^{3+,4+}O_4$ and $Mn^{4+}O_2$ (pyrolusite), and at 641.6 eV for Mn^{3+} in $LiMn_2{}^{3+,4+}O_4$ and $Mn_2{}^{3+}O_3$ (bixbyite) [34]. In this case, the two peaks of Mn2p ($Mn2p^{3/2}$ and $Mn2p^{1/2}$) are located at 642.2 and 653.8 eV, respectively, with an energy separation of 11.6 eV. It is obvious that the binding energy of $Mn2p^{3/2}$ peak is intermediate between those of Mn^{4+} (642.6 eV). The peak positions and the intensity ratio of $Mn2p^{3/2}$ and $Mn2p^{1/2}$ show that $LiMn_2O_4$ exists in the form of a stoichiometric spinel. The peaks of O1s for both materials appear at 529.7 eV, which reflects the presence of O elements in the state of O^{2-}.

3.3. Raman analysis

The Raman spectra of the two materials in the spectral region of 200–2000 cm^{-1} were obtained (Fig. 6). Common features of these spectra are the presence of a strong band at around 650 cm^{-1} and a group of bands between 200 and 500 cm^{-1} with a lower intensity. For spinel oxides and other manganese oxides, energies at ~650 cm^{-1} are characteristic of vibrations that involve the motion of oxygen atoms inside the octahedral MnO_6 unit [35]. The weak Raman scattering efficiency is attributed to the electronic properties of $LiMn_2O_4$. The assignment of Mn–O bands confirms that the $LiMn_2O_4$ spinel structure is successfully formed after calcination at a low temperature of 250 °C. The spectrum corresponding to the MWCNT-$LiMn_2O_4$ composite (Fig. 6b) suggests that the M–O bands of the composites are marginally shifted to higher frequencies than the $LiMn_2O_4$ nanoparticles. There are two main peaks arising from

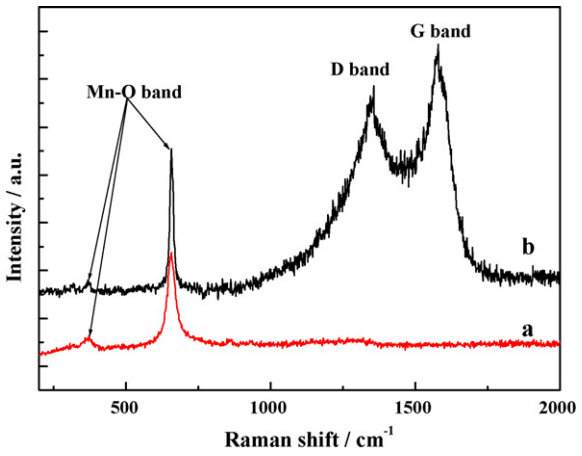

Fig. 6. Raman spectra of samples (a) $LiMn_2O_4$ and (b) MWCNT-$LiMn_2O_4$ nanocomposites.

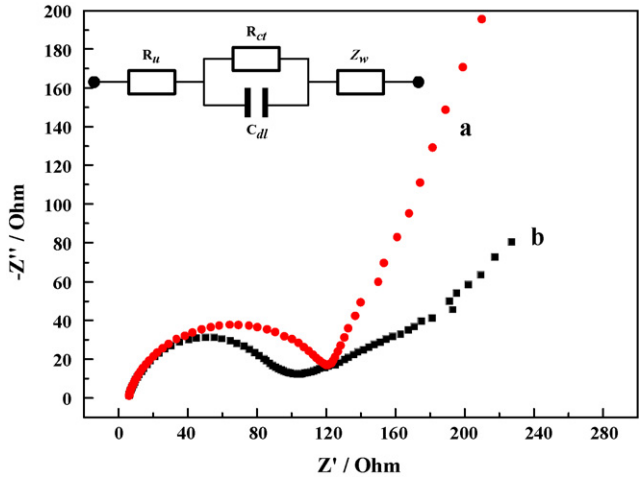

Fig. 8. Impedance spectra of samples. Inset is equivalent circuit used to fit impedance data. (a) Without MWCNTs and (b) with MWCNTs.

the presence of MWCNTs at around 1336 and 1570 cm^{-1}, known as the D-band and G-band of graphite, respectively. The D-band corresponds to the sp^3 structural disorder due mainly to defects in the curved graphene sheets and tube ends, whereas the G-band reflects the structural integrity of the sp^2-hybridized graphene sheets [36,37].

3.4. Electrochemical performance

The electrochemical properties of the cathode materials were evaluated by using 2032 coin-type cells. Representative charge–discharge curves are shown in Fig. 7a. The cells were cycled at a current density of 2*C* (where $C = 148\ mAh\ g^{-1}$) between 3 and 4.3 V. The curves exhibit two close pseudo plateaux at around 4.0 V, which is a typical profile for the electrochemical extraction and insertion of lithium ions. This result confirms two equilibrium binary systems during Li^+ intercalation into the $LiMn_2O_4$ electrode. It is noted that the MWCNT-$LiMn_2O_4$ nanocomposites show a much higher capacity than the $LiMn_2O_4$ nanoparticles. The smaller polarization of the MWCNT-$LiMn_2O_4$ nanocomposite electrode is contrasted with that of $LiMn_2O_4$ nanoparticles during charge–discharge cycles. Fig. 7b compares the cyclic performance of the two electrodes at the 2*C* rate with a cut-off voltage of 3.0–4.3 V (versus Li/Li^+) at room temperature. Both the initial discharge capacity and the cyclic performance of the MWCNT-$LiMn_2O_4$ electrode are superior to those of the $LiMn_2O_4$ electrode. The $LiMn_2O_4$ electrode has an initial discharge capacity of 54.7 $mAh\ g^{-1}$, with a 9% loss of the initial capacity after 20 cycles. By contrast, the discharge capacity of the composite electrode is 66.5 $mAh\ g^{-1}$ and over 99% of this capacity is retained after 20 cycles; the loss is about 4% even after 100 cycles. The electrochemical performance of electrodes, especially the cyclic performance, is directly related to the robustness of their electrical contact. A higher electronic conductivity of spinel $LiMn_2O_4$ electrodes corresponds to a higher cycle performance [38]. The excellent electrical conductivity of MWCNTs and the hybridization with the active material are mainly responsible for the superior cyclic performance of the MWCNT-$LiMn_2O_4$ electrodes. The MWCNTs act as intra-electrode wires, there by facilitating charge-transfer among the spinel $LiMn_2O_4$ particles.

The electrochemical impedance spectra (EIS) of spinel $LiMn_2O_4$ nanoparticles with and without MWCNT reinforcements are shown in Fig. 8. The EIS data were collected with a two-electrode coin cell after activation (i.e., after subjecting the coin cell to one charge–discharge cycle). The initial activation was aimed to suppress the Li–electrolyte interfacial resistance that arises from the passivating film formed on lithium metal in contact with the electrolyte. The Nyquist plots are typically represented by a semicircle followed by a sloping, straight line at low frequencies. The impedance spectra can be explained on the basis of an equivalent circuit with uncompensated resistance (R_u), charge-transfer resistance (R_{ct}), double-layer capacitance (C_{dl}), and Warburg impedance (Z_w). The uncompensated resistance is the resistance between the

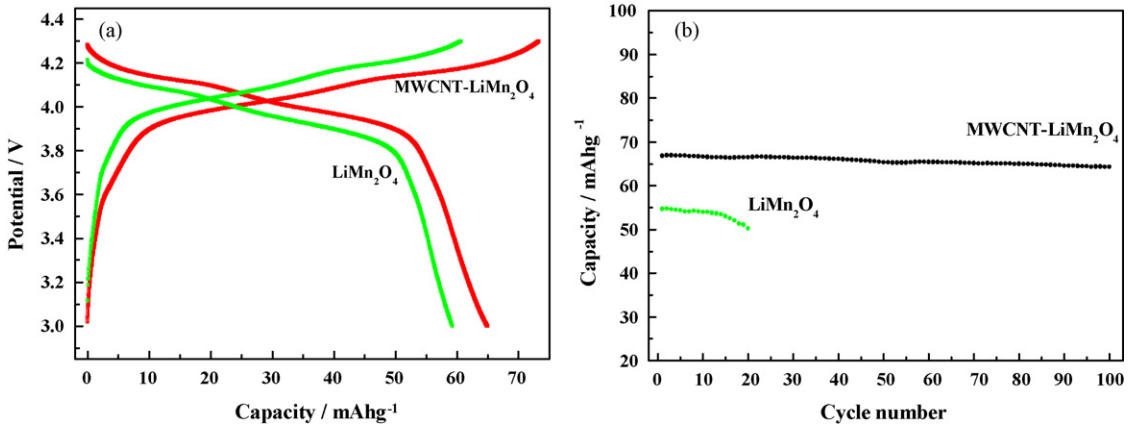

Fig. 7. (a) Galvanostatic charge–discharge curves of samples at 2*C* rate and (b) residual discharge capacity versus cycle number at the rate of 2*C*.

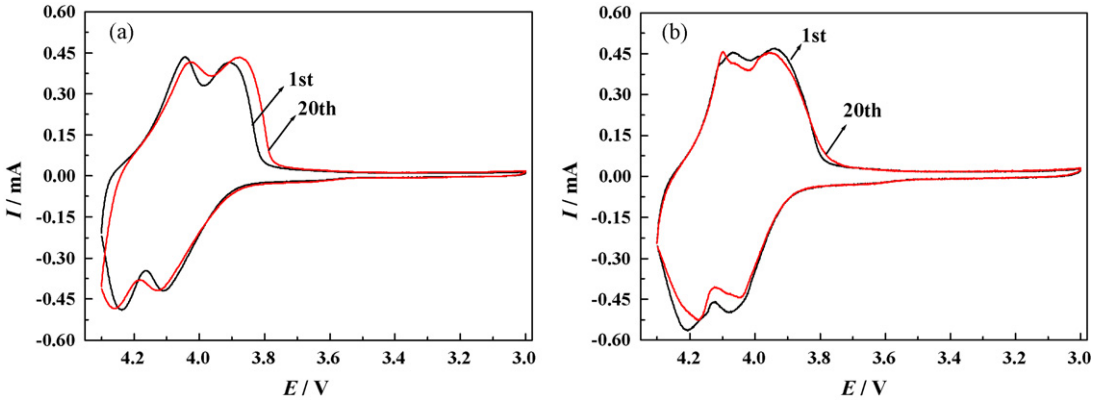

Fig. 9. Cyclic voltammetric curves for (a) $LiMn_2O_4$ nanoparticles and (b) MWCNT-$LiMn_2O_4$ nanocomposite electrodes at scan rate of 0.2 mV s^{-1}.

electrode and the current-collector. The diameter of the semicircle in Fig. 8 corresponds to the charge-transfer resistance (R_{ct}), which is related to the electrochemical reaction at the electrode|electrolyte interface and particle–particle contact. A large semicircle means a high charge-transfer resistance. The sloping line in the very low frequency region is attributed to the Warburg impedance (Z_W), which is associated with Li ion diffusion in the bulk of the active material. A significant reduction in charge-transfer resistance from 120.4 Ω for the spinel $LiMn_2O_4$ to 98.3 Ω for the MWCNT-$LiMn_2O_4$ nanocomposite is a direct indication of the improved electrical conductivity arising from the intimate networking of MWCNTs with $LiMn_2O_4$ nanoparticles which, in turn, facilitates a faster charge-transfer between the $LiMn_2O_4$ nanoparticles. This observation is consistent with the change in the charge–discharge profile, as discussed above.

The typical cyclic voltammetric curves (CVs) for the two electrodes are presented in Fig. 9. The oxidative peaks of $LiMn_2O_4$ nanoparticles on the 1st cycle occur at 4.04 and 4.17 V, and the reductive peaks at 3.95 and 4.07 V. These values are consistent with reported data [17,39] and are the same as those in the CVs of the MWCNT-$LiMn_2O_4$ nanocomposite (Fig. 9b). The corresponding peaks on the 20th cycle of the nanoparticles are shifted from those of the 1st cycle and therefore suggest that the surface structure of the nanoparticles is initially less crystalline or defective. When the two cathode materials are compared, the $LiMn_2O_4$ nanoparticles in general exhibit lower reversibility than the MWCNT-$LiMn_2O_4$ nanocomposites. The CVs for the MWCNT-$LiMn_2O_4$ nanocomposite have similar positions and intensities of peak currents for both anodic and cathodic curves on the 1st and 20th cycles. The potential difference (DE_p) of the two redox peaks is approximately 0.09 and 0.14 V for the 1st and 20th cycles, respectively. This confirms the excellent reversibility at room temperature due to the introduction of MWCNTs.

The charge–discharge curves of the MWCNT-$LiMn_2O_4$ composite at different rates of 0.1, 0.5, 1, 2, 8 and 13*C* at room temperature are shown in Fig. 10. As expected, the discharge capacity decreases with increasing charge rate; the corresponding discharge capacities are 72, 70, 67, 63, 55 and 31 mAh g^{-1}, respectively. These values are determined at higher charge–discharge rates of 0.5, 1, 2, 8, and 13*C*, respectively, which correspond to approximately 97, 93, 87, 76 and 43% of the discharge capacity obtained at 0.1*C*. The large potential drops in the charge–discharge curves of the MWCNT-$LiMn_2O_4$ composites result from the *iR* drops of the lead line and cell structure of a two-electrode cell at high charge–discharge rates.

The MWCNT-$LiMn_2O_4$ nanocomposite cathodes exhibit excellent cycleability and reversibility. Fig. 11 shows the residual specific discharge capacity versus cycle number when the electrodes are subjected to 5 sets of 10 cycles at the same rate. An important observation is that the reduction in discharge capacity after each set of

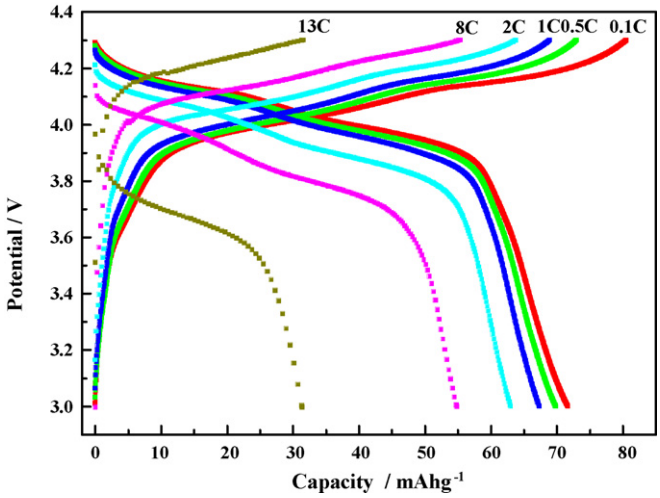

Fig. 10. Charge–discharge curves of MWCNT-$LiMn_2O_4$ nancomposite at different current rates.

10 cycles is remarkably low, i.e., 2.6, 1.5, 1.4, 1.2 and 6.5% at an increasing rate of 0.5, 1, 2, 8 and 13*C*, respectively. These degradation rates are considered to be very low, especially when the rate is lower than 8*C*. This observation demonstrates that the structure of the composite is very stable and the electrochemical Li^+ insertion/extraction process is quite reversible even at a rate as high as 8*C*. Although the discharge capacity of the $LiMn_2O_4$ phase prepared

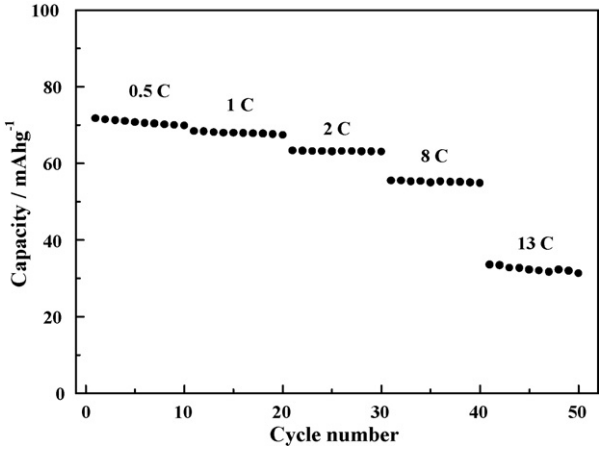

Fig. 11. Specific discharge capacities versus cycle number for nanocomposite cathode at different current rates.

at a low temperature is relatively low compared with that of the spinel phase $LiMn_2O_4$ prepared at over 700 °C (~125 mAh g^{-1}), the initial open-circuit voltage of 3.4 V and the two potential plateaux in the 4 V range obtained in this study are typical properties for spinel $LiMn_2O_4$. These findings partly confirm the successful preparation of MWCNT-$LiMn_2O_4$ nanocomposites using the facile sol–gel method.

4. Conclusions

MWCNT-$LiMn_2O_4$ nanocomposites have been synthesized using the sol–gel method, followed by calcination at 250 °C. Both the low-temperature heat treatment and the chemical lithiation process could form crystalline $LiMn_2O_4$ nanoparticles mixed with MWCNTs. Compared with spinel $LiMn_2O_4$ nanoparticles, the as-synthesized MWCNT-$LiMn_2O_4$ nanocomposites show a high charge–discharge capability and an excellent cycleability as well as high reversibility as cathode materials for LIBs. The role of MWCNTs in the cathode materials is to facilitate fast transportation and intercalation kinetics of Li ions. Furthermore, the method developed in this study opens up a new prospect for high-yield synthesis of hybrid nanocomposites for LIBs.

Acknowledgements

This project was supported by the FINETEX-HKUST R & D Center (Project code: FTG001-MECH.07/08) and the Innovation and Technology Fund of Hong Kong SAR (Project code: GHP/028/08SZ). The authors are also grateful for the technical assistance from the Materials Characterization and Preparation Facilities (MCPF) of HKUST and Dr. Baohua Li from Tsinghua University in PR China.

References

[1] M. Armand, J.M. Tarascon, Nature 451 (2008) 652–657.
[2] P.G. Bruce, B. Scrosati, J.-M. Tarascon, Angew. Chem. Int. Ed. 47 (2008) 2930–2946.
[3] K. Raveendranath, J.R.S. Jayalekshmi, T.M.A. Rasheed, K.P.R. Nair, Mater. Sci. Eng. B 131 (2006) 210–215.
[4] N. Amdouni, F. Gendron, A. Mauger, H. Zarrouk, C.M. Julien, Mater. Sci. Eng. B 129 (2006) 64–75.
[5] J.M. Tarascon, D. Guyomard, Electrochim. Acta 38 (1993) 1221–1231.
[6] M. Molenda, R. Dziembaj, E. Podstawka, W. Lasocha, L.M. Proniewicz, J. Phys. Chem. Solids 67 (2006) 1347–1350.
[7] Y.-P. Fu, C.-H. Lin, Y.-H. Su, S.-H. Wu, J. Power Sources 159 (2006) 215–218.
[8] S.-W. Lee, K.-S. Kim, H.-S. Moon, J.-P. Lee, H.-J. Kim, B.-W. Cho, W.-I. Cho, J.-W. Park, J. Power Sources 130 (2004) 227–232.
[9] J.-S. Chen, L.-F. Wang, B.-J. Fang, S.-Y. Lee, R.-Z. Guo, J. Power Sources 157 (2006) 515–521.
[10] H.-W. Chan, J.-G. Duh, S.-R. Sheen, S.-Y. Tsai, C.-R. Lee, Surf. Coat. Technol. 200 (2005) 1330–1334.
[11] D. Shu, G. Kumar, K.-B. Kim, K.S. Ryu, S.H. Chang, Solid State Ionics 160 (2003) 227–233.
[12] Y. Xia, T. Sakai, T. Fujieda, X.Q. Yang, X. Sun, Z.F. Ma, J. McBreen, M. Yoshio, J. Electrochem. Soc. 148 (2001) A723–A729.
[13] M. Takahashi, T. Yoshida, A. Ichikawa, K. Kitoh, H. Katsukawa, Q. Zhang, M. Yoshio, Electrochim. Acta 51 (2006) 5508–5514.
[14] Y. Xia, Y. Zhou, M. Yoshio, J. Electrochem. Soc. 144 (1997) 2593–2600.
[15] A. Paolone, R. Cantelli, B. Scrosati, P. Reale, M. Ferretti, C. Masquelier, Electrochem. Commun. 8 (2006) 113–117.
[16] B. Denga, H. Nakamura, Q. Zhang, M. Yoshio, Y. Xia, Electrochim. Acta 49 (2004) 1823–1830.
[17] X. Li, Y. Xu, Electrochem. Commun. 9 (2007) 2023–2026.
[18] J. Cho, J. Mater. Chem. 18 (2008) 2257–2261.
[19] D.K. Kim, P. Muralidharan, H.-W. Lee, R. Ruffo, Y. Yang, C.K. Chan, H. Peng, R.A. Huggins, Y. Cui, Nano Lett. 8 (2008) 3948–3952.
[20] E. Hosono, T. Kudo, I. Honma, H. Matsuda, H. Zhou, Nano Lett. 9 (2009) 1045–1051.
[21] G. Wang, Q. Zhang, Z. Yu, M. Qu, Solid State Ionics 179 (2008) 263–268.
[22] X. Li, F. Kang, W. Shen, Electrochem. Solid-State Lett. 9 (2006) A126–A129.
[23] X. Li, F. Kang, W. Shen, Carbon 44 (2006) 1298–1352.
[24] K. Sheem, Y.H. Lee, H.S. Lim, J. Power Sources 158 (2006) 1425–1430.
[25] B. Jin, H.B. Gu, W. Zhang, K.H. Park, G. Sun, J. Solid State Electrochem. 12 (2008) 1549–1554.
[26] X. Li, F. Kang, X. Bai, W. Shen, Electrochem. Commun. 9 (2007) 663–666.
[27] L. Wang, Y. Huang, R. Jiang, D. Jia, J. Electrochem. Soc. 154 (2007) A1015–A1019.
[28] S. Liu, J. Zhang, K. Huang, J. Yu, J. Braz. Chem. Soc. 19 (2008) 1078–1083.
[29] Y. Shan, L. Gao, Chem. Lett. 33 (2004) 1560–1561.
[30] J. Li, S. Tang, L. Lu, H.C. Zeng, J. Am. Chem. Soc. 129 (2007) 9401–9409.
[31] G. Chen, Z. Wang, D. Xia, Chem. Mater. 20 (2008) 6951–6956.
[32] Y. Geng, M.Y. Liu, J. Li, X.M. Shi, J.K. Kim, Compos. Part A 39 (2008) 1876–1883.
[33] Y. Geng, J. Li, S.J. Wang, J.K. Kim, J. Nanosci. Nanotechnol. 8 (2008) 6238–6246.
[34] N. Treuil, C. Labrugere, M. Menetrier, J. Portier, G. Gampet, A. Deshayes, J.C. Frison, S.J. Hwang, S.W. Song, J.H. Choy, J. Phys. Chem. B 103 (1999) 2100–2106.
[35] C.V. Ramana, M. Massot, C.M. Julien, Surf. Interface Anal. 37 (2005) 412–416.
[36] P.C. Ma, J.K. Kim, B.Z. Tang, Carbon 44 (2006) 3232–3238.
[37] Y. Geng, S.J. Wang, J.K. Kim, J. Colloids Interface Sci. 336 (2009) 592–598.
[38] J.T. Son, H.G. Kim, J. Power Sources 147 (2005) 220–226.
[39] F.O. Ernst, H.K. Kammler, A. Roessler, S.E. Pratsinis, W.J. Stark, J. Ufheil, P. Novák, Mater. Chem. Phys. 101 (2007) 372–378.